Comparison of the physicochemical properties and aging behavior of two different APTES-derived plasma polymer-based coatings

Tim Egghe[1,2,*,], Mehrnoush Narimisa[1,*], Rouba Ghobeira[1], Bernard Nisol[1,3], Yuliia Onyshchenko[1], Richard Hoogenboom[2], Rino Morent[1], Nathalie De Geyter[1]**

[1]Research Unit Plasma Technology (RUPT), Department of Applied Physics, Faculty of Engineering and Architecture, Ghent University, Sint-Pietersnieuwstraat 41 B4, 9000 Ghent, Belgium

[2]Supramolecular Chemistry Group, Centre of Macromolecular Chemistry (CMaC), Department of Organic and Macromolecular Chemistry, Faculty of Sciences, Ghent University, Krijgslaan 281 S4, 9000 Ghent, Belgium

[3]Molecular Plasma Group (MPG), Foetz, Luxembourg

* Both authors equally contributed to the manuscript

**Corresponding author: tim.egghe@ugent.be

Abstract

Recently, new plasma polymerization-based techniques emerged to deposit chemically functional coatings for various applications. However, little is known on the aging of these layers. Therefore, this study aims to investigate the physicochemical properties of aerosol-assisted atmospheric pressure plasma deposited (3-aminopropyl)triethoxysilane-based (AAPD-APTES) coatings and compare their aging behavior to APTES-modified plasma polymerized hexamethyldisiloxane-based coatings (ppHMDSO-APTES). X-ray photoelectron spectroscopy (XPS), attenuated total reflection-Fourier transform infrared spectroscopy (ATR-FTIR), water contact angle (WCA) and atomic force microscopy (AFM) measurements indicated that the applied power had an insignificant impact on the wettability, chemistry and morphology of the AAPD-APTES films. A complex nitrogen-containing organosilicon layer was obtained with significant preservation of the Si-O-C-bonds. For the ppHMDSO-APTES coatings, XPS indicated that these layers had a significantly higher amount of preserved primary amines and a different surface morphology. Oxidation and hydrolysis of Si-O-C-bonds were the most prevalent aging processes for the AAPD-APTES coatings, while protonation of primary amines was most important for the ppHMDSO-APTES films. This study indicates that further research is needed to examine the differences in coating chemistry and aging of other AAPD-based and conventional plasma polymers. Additionally, it provides a reference to decide which coating type and associated aging processes are preferred for certain applications.

Keywords: plasma polymerization, aerosol-assisted atmospheric pressure plasma deposition, plasma-enhanced chemical vapor deposition, (3-aminopropyl)triethoxysilane, aging

1. Introduction

In the last decades, plasma polymerization emerged as an attractive technique for surface modification because of its advantages over a variety of conventional techniques.[1-2] Usually, plasma polymerization refers to the deposition of cross-linked, sub-micrometer coatings by introducing organic compounds (often called precursors or monomers) in a non-thermal plasma.[3-4] A variety of different types of plasma polymerization exist, among which plasma-enhanced chemical vapor deposition (PECVD) is the most investigated type.[1] Other prominent plasma polymerization types are liquid- or aerosol-assisted atmospheric pressure plasma deposition (AAPD) and magnetron sputtering-based PECVD.[5-6] A main challenge for plasma polymerization methods is to preserve the monomer functionality in the resulting coating, as the interaction between the monomer and plasma results in precursor fragmentation.[3, 7] In order to synthesize coatings with a specific chemical functionality, which were previously referred to as "selective functional plasma polymer coatings", multiple studies have employed a modification step after plasma polymer deposition.[2] This can be useful for certain applications like biosensors or antibacterial coatings. Friedrich *et al.,* for example, developed a two-step method that was based on the deposition of bromine-based plasma polymer coatings, after which diamines, diols, dithiols or sodium azides can react with the C-Br bond to form coatings with a high density of amine, alcohol, thiol and azide functionalities, respectively.[8-10] More recently, plasma polymerized hexamethyldisiloxane (ppHMDSO) coatings were silanized with (3-aminopropyl)triethoxysilane (APTES) and (3-bromopropyl)trichlorosilane (BrPTCS) to obtain coatings with a high density of primary amines and alkyl bromides.[2] The main advantage of this method is that the ppHMDSO coating can be deposited on any surface to make them suitable for further silanization reactions. Additionally, other functionalities can be introduced by this technique due to the wide variety of available commercial silanization agents.

A particular challenge in the design of plasma polymer coatings, besides optimizing the functional group density, is the reduction of aging phenomena in air and water.[11] Indeed, different processes, such as post-plasma oxidation caused by trapped near-surface free radicals, post-plasma surface restructuring and reactions between the surrounding media and the unstable chemical functionalities in the film, are contributing to changes in the coating chemistry over time.[11] For plasma polymers synthesized by PECVD, aging phenomena and strategies to avoid aging are relatively well-studied, as summarized by Vandenbossche and Hegemann.[11] However, little is known on the aging of more recently emerging plasma polymer coatings, such as AAPD-based and selective functional plasma polymer coatings.

Therefore, this study aims to examine and compare the aging of AAPD-based coatings and ppHMDSO-based selective functional plasma polymers in air. To allow a proper comparison, APTES is selected as the precursor for AAPD and as the silanization agent for the ppHMDSO coating, as it is one of the most used silanization agents and is also frequently employed as precursor for both PECVD and AAPD.[12-16] APTES-based, and other aminosilane-based (like (3-aminopropyl)trimethoxysilane (APTMS)) plasma polymers can be used for a variety of applications like tribological coatings, the immobilization of biomolecules or nanoparticles via coupling with the primary amine group (which can be used for various applications like sensors, antibacterial coatings and catalytic surfaces), the improvement of adhesiveness between substrates and an epoxy resin, and the promotion of cell growth, among others.[13, 15-19] Despite their wide-spread usage, the aging of these coatings is only studied to a very limited extent for PECVD.[20]

The aim of this paper is threefold. Firstly, the wettability, surface chemistry and morphology of the AAPD-based APTES (AAPD-APTES) coatings is investigated as a function of power, as it is known to be one of the main factors that can influence the chemistry and aging behavior in air for PECVD-based coatings.[11, 21-23] Secondly, the wettability, surface chemistry and morphology of the APTES-modified ppHMDSO (ppHMDSO-APTES) is compared to the AAPD-APTES coatings, which can reveal the influence of the plasma-precursor/coating interactions on the surface chemistry, among others. Lastly, the aging of AAPD-APTES and ppHMDSO-APTES coatings is examined and compared by investigating the surface wettability and chemistry changes upon air exposure for several days. The surface

chemistry is investigated by X-ray photoelectron spectroscopy (XPS) and attenuated total reflection-Fourier transform infrared spectroscopy (ATR-FTIR), while the surface wettability and morphology are studied by water contact angle (WCA) measurements and atomic force microscopy (AFM), respectively.

2. Materials and methods

2.1. Materials

Ethanol 96 % (EtOH) (denaturated), acetone (99.5%) and toluene (≥ 99.5%) were purchased from Carl Roth. APTES (99%) was purchased from Merck, while HMDSO (≥ 98%) was purchased from Acros Organics. Helium (He) (purity: 99.999%) and nitrogen (N_2) (purity: ≥ 99.999%) were purchased from Air Products and Air Liquide, respectively. All chemicals and gasses were used as supplied. A roll of ultra-high-molecular-weight polyethylene (UHMWPE) (thickness: 0.075 mm) film was obtained from Goodfellow. Silicon (Si) wafers (diameter of 10.2 cm) were purchased from Siegert Wafer GmbH and cut into smaller parts before deposition. Si and UHMWPE were used as deposition substrate without any pre-treatment.

2.2. Coating deposition

2.2.1. AAPD-APTES

In this study, a PlasmaSpot® 500 (Molecular Plasma Group (MPG), Luxembourg) dielectric barrier discharge (DBD) plasma jet was used. This R&D system enables the generation of atmospheric pressure cold (near ambient T) plasmas. It consists of two concentric tubular electrodes; the external one is covered with a dielectric layer and is connected to the power source, while the inner one is grounded. The system is designed so that the plasma gas travels through the electrode gap, and the chemical precursors are carried by the same type of gas inside the inner tube (see***Figure 1*.** **Schematic representation of the MPG's PlasmaSpot® 500.Figure 1**). This enables very mild activation of precursors that are only plasma-activated in the afterglow, and prevents the undesirable deposition of coatings on surfaces in the electrode gap. The precursor is fed to the system as aerosols (sub-micrometric scale), which are generated by a nebulizer that is based on the Venturi effect, as described before.[24]

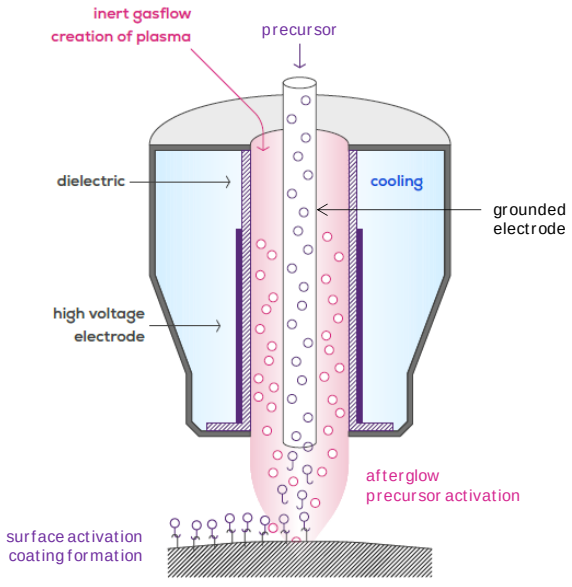

Figure 1. Schematic representation of the MPG's PlasmaSpot® 500.

The PlasmaSpot® powered electrode was fed with a high-voltage up to 15 kV_{p-p}, at a frequency in the 50-60 kHz range. Plasma (and carrier) gas used in this study was nitrogen. Using this gas, the nominal output (or applied) power range was 150-450 W. The discharge gas was fed into the system at a fixed flow rate of 80 standard liter per minute (slm), whereas the atomizing and dilution flows of nitrogen that were used for APTES nebulization were set at 0.75 slm and 5 slm, respectively. The UHMWPE samples were cut as strips of 15×50 mm^2 and 8 strips were stuck to a wooden slab. UHMWPE was used as substrate because of its low interference in the ATR-FTIR spectra. The device was moved over the entire sample surface using a moving stage with 2.04 m/min velocity and a track width of 5 mm. The device passed 6 times over all UHMWPE samples. The distance between the edge of the capillary and the sample was fixed at 18 mm. Three different plasma input powers (150, 185, 220 W) were selected to obtain a thorough insight into the influence of this parameter on the coating characteristics. Above 220 W, the substrates started deforming upon the treatment because of an increased plasma temperature.

2.2.2. ppHMDSO-APTES

The APTES modification of the ppHMDSO coatings was performed in a similar way as previously described.[2, 25] An elaborate description of the used plasma reactors and reaction conditions can be found in a previous study.[25] In short, PDMS-like ppHMDSO coatings were deposited by a medium-pressure DBD reactor on UHMWPE substrates (size of 1 cm x 2.5 cm, approximately). The DBD set-up operated at 10 kPa and used 1000 standard cubic centimeters per minute (sccm) of He as carrier gas, while the precursor was introduced in the reactor with a bubbling system at a rate of 9.3 mg/min. The treatment was performed for 1 min at an applied power of 0.8 W, which was calculated as previously described.[25] After the plasma polymerization, the ppHMDSO-modified UHMWPE substrates were removed from the reactor and subsequently plasma activated in a separate DBD reactor by using dry air at a flow of 1000 sccm at a pressure of 5 kPa. The treatment time was 5 s and the applied power 2.7 W. This treatment resulted in the introduction of silanol groups on the ppHMDSO surface, which were necessary to enable an efficient APTES silanization.[2] After the plasma activation, the sample was transferred within 3 min to a reaction flask containing 5 ml of toluene at 70°C, after which the respective amount of APTES (2% v/v) was added. The mixture was stirred for 1 hour, followed by the sample removal. This reaction time was necessary to reach a surface chemistry saturation, as indicated in a previous study.[2] For WCA analysis, the sample was washed with ethanol and dried with dry air to allow a direct wettability evaluation, while the samples for AFM, XPS and ATR-FTIR analysis were stored in vacuum before examination.

2.3. AFM

The influence of the different steps in the coating fabrication on the surface morphology and roughness has been investigated by AFM. All measurements were performed by an XE-70 atomic force microscope (Park Systems), operating in the non-contact mode and using a silicon cantilever with a spring constant of 40 N/m (Nanosensors™ PPP-NCHR). The scan size used for all the measurements was 45 × 45 μm^2. XEI software was used for surface roughness analysis after the recorded images were modified by line leveling in the X-axis direction. For each condition, three samples with three different regions of interest on each sample were investigated. Root mean square roughness (Rq) values are presented as the average over these 9 measurement points.

2.4. WCA analysis

The wettability of different coatings was analyzed by WCA measurements using a commercial Krüss Easy Drop system at room temperature. After the AAPD process, between 7 and 9 deionized water droplets of 2.0 µl were placed on different positions of a strip. In total, 5 strips obtained from 3

different plasma experiments were analyzed, resulting in 40 WCA values. The results are presented as average ± standard deviation. For the ppHMDSO, air plasma activated ppHMDSO and ppHMDSO-APTES samples, 2-5 droplets (depending on the wettability) were deposited on each strip and these measurements were performed in triplicate. WCA values were measured within 10 minutes after coating deposition or plasma activation process for all these samples. For the aging experiments, at least 25 and 12 droplets, for the AAPD- and ppHMDSO-APTES samples, respectively, were examined for each condition at the respective aging times. The WCAs were measured on three strips, which were synthesized in three different plasma experiments.

2.5. XPS

XPS surface analysis was performed on a PHI 5000 Versaprobe II spectrometer, using a monochromatic Al K_α X-ray source (hv = 1486.6 eV) operating at 25 W. A vacuum of at least 10^{-6} Pa was maintained during all measurements. Survey scans and high-resolution spectra (C1s, N1s, O1s, Si2p) were recorded with pass energies of 187.85 eV (eV step = 0.8 eV) and 23.50 eV (eV step = 0.1 eV), respectively, with a take-off angle of 45° and a spot diameter of 100 µm. Multipak (v9.6.1) was used for elemental analysis using a Shirley background and the relative sensitivity factors supplied by the manufacturer. The calibration of high-resolution XPS spectra was performed in Multipak by shifting the peak of the C1s spectra to 285.0 eV (C-C bond). For a qualitative comparison of the high-resolution XPS spectra, the binding energies were obtained from literature and displayed on the spectra. A summary can be found in **Table 1**.[9, 26-28] SiO_x will be further used to indicate a silicon connected to X O's and (4-X) C's. It should be noted that the attribution of some bonds in C1s and N1s binding energies is somewhat ambiguous in aminosilane-based films.[29] Therefore, the assigned energies were limited to the ones that were confirmed during previous measurements with the XPS equipment used in this work.[2-3, 7, 30] In the C1s spectra, amides were located at 287.7 eV, selected as the average of the energy range observed before for amides (287.4 – 288.0 eV).[3] In the N1s spectra, amides were located at 399.8 eV in this work, but previous measurements already indicated that there was a range in which the peak of the contribution of this functionality can be found (399.6 – 400.0 eV).[3, 30] Protonated amines were found to have a contribution at 400.9 eV before, but also this functionality was reported to result in contributions over a wide range of energies (400.6 – 401.9).[28] For the N1s spectra, other N-containing functionalities were either displayed without a designated energy (like imines and (iso)nitriles) or discussed in the text. For all samples, a part of approximately 1 cm x 1 cm was cut out of the treated UHMWPE strips and 4 points were measured per sample. For the aging measurements, it should be noted that small variations exist for different measurement points on one sample. But the conclusions that are made in the paper remain valid for all the different analyzed spots, as these variations just relate to minimal differences in the extent in which protonation and/or oxidation occurred.

Table 1.Binding energies used for the qualitative analysis of high-resolution XPS spectra.

C1s		Si2p		N1s	
Bond	**Binding energy (eV)**	**Bond**	**Binding energy (eV)**	**Bond**	**Binding energy (eV)**
C-Si	284.4	SiO	101.5	$C\text{-}NH_2$	399.3
C-C	285.0	SiO_2	102.1	Amide	399.8
C-N	285.7	SiO_3	102.8	$C\text{-}NH_3^+$	400.9
C-O	286.6	SiO_4	103.4		
C=O/N-C=O	287.7				
COOH/COOC	288.9				

2.6. ATR-FTIR

A Bruker Tensor 27 spectrometer equipped with a single reflection attenuated total reflectance accessory (MIRacle, Pike technology) was used to perform FTIR analysis on coated UHMWPE substrates, using a germanium crystal as the internal reflection element. All spectra were acquired using a mercury cadmium telluride (MCT) detector (liquid N_2 cooled) in the spectral region of 4000-700 cm^{-1}, and 64 scans (resolution 4 cm^{-1}) were made for each sample. OPUS 7 software was used to analyze the obtained spectra and correct for the presence of CO_2 peaks within the spectra originating from the ambient environment. In order to ensure the reliability of the results, each of the analyses was conducted on three spots for three different samples (9 points per condition in total). The measurements were conducted within 15 min after the coating deposition was finished.

3. Results and discussion

3.1. Influence of power on the physicochemical properties of AAPD-APTES coatings

Before the AAPD-APTES coatings were studied on the UHMWPE substrate, a couple of preliminary experiments were conducted to optimize the deposition process. The main gas flow, dilution flow, the distance from sample to jet outlet, and the movement parameters were set to typically used values with the employed plasma set-up, and the atomizing flow was varied at a power of 150 W. From this, it was observed that 0.75 slm of atomizing flow resulted in the formation of coatings on UHMWPE and Si wafers that showed a relatively flat morphology without the presence of a significant amount of droplet deposition. Therefore, 0.75 slm was selected as atomizing flow, after which the power was varied. As mentioned before, the influence of the applied power is examined as it is known to be one of the main factors that can influence the chemistry and morphology of PECVD-based coatings.[11, 21-23] Above 220 W, the substrates started deforming upon treatment because of an increased plasma temperature. Therefore, three powers were selected in the range of 150 to 220 W to evaluate possible trends as a function of power (150, 185 and 220 W). To get insight in the nature of the AAPD-APTES coatings before the physicochemical and aging evaluation, the layers were rinsed with deionized water and incubated for 15 min in deionized water. Figure S1 in the Supplementary data shows the AAPD-APTES coatings on Si wafers for the different investigated powers before and after the water rinsing and incubation. From this figure, it can be observed that the different AAPD-APTES coatings can withstand the rinsing and incubation process, showing that the layers have a certain degree of cross-linking and stability. Thus, it is clear that an APTES-based plasma polymer is deposited by the AAPD process, and these different coatings were further investigated by AFM, WCA, XPS and ATR-FTIR measurements in the following sections.

3.1.1. AFM

The surface morphology of the coatings was examined using AFM as the AAPD-APTES procedure could alter the surface morphology of the produced samples. **Figure 2** shows a representative image of the surface morphology and the determined root mean square roughness (R_q) value for the different AAPD-APTES samples in comparison to the uncoated UHMWPE substrate. As illustrated in the figure, the pristine UHMWPE reveals an R_q value of 166.9 ± 74.5 nm, suggesting that the substrate itself has a rather rough structure with variations over the sample surface, resulting in a high standard deviation. The AFM images of the different AAPD-APTES coatings show that the surface morphology of these samples is similar to the UHMWPE substrate, as shown in **Figure 2.B, C, and D**. This indicates that the thickness of the deposited coatings is smaller than the substrate roughness and that it is mainly the substrate that determines the overall surface morphology. However, the coated samples have a slightly higher R_q value as compared to the uncoated UHMWPE. This seems to be in line with the

introduction of some additional features on the surface. This could be caused by the introduction of particulates into the coating, originating from cross-linked aerosol droplets due to the interaction with the plasma.[31-32] No significant differences between the AAPD-APTES coatings deposited at different powers could be observed. The R_q value of the film deposited at 185 W shows a slight but non-significant variation in comparison to the other two conditions. As such, it can be concluded that the applied power did not have a significant effect on the surface morphology within the employed power range.

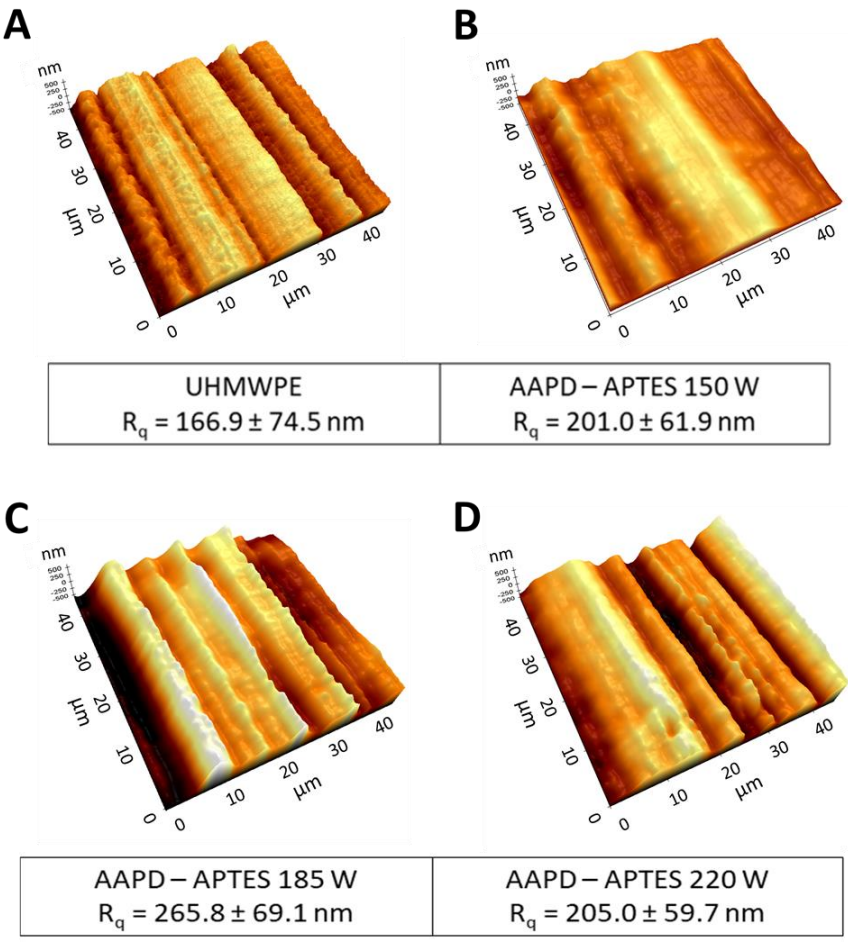

Figure 2. AFM 3D images and root mean square roughness values for UHMPWE and AAPD-APTES coatings deposited at different powers.

3.1.2. WCA and XPS

The wettability and surface chemistry of AAPD-APTES coatings as a function of power were examined by WCA and XPS, respectively. **Table 2** summarizes the wettability and atomic composition obtained by XPS measurements of the UHMWPE substrate and AAPD-APTES coatings deposited at 150, 185 and 220 W. Reference values are added to allow a more thorough analysis.

Table 2. WCAs and XPS atomic composition for UHMWPE and AAPD coatings deposited at 150, 185 and 220 W.

	WCA (°)	XPS atomic composition			
		C%	O%	Si%	N%
UHMWPE	113.6 ± 2.1	99.2 ± 0.2	0.8 ± 0.2		

AAPD-150 W	62.2 ± 1.5	55.4 ± 0.4	28.7 ± 0.6	9.4 ± 0.3	6.5 ± 0.4
AAPD-185 W	64.6 ± 1.7	56.1 ± 0.5	28.2 ± 0.4	9.5 ± 0.4	6.3 ± 0.5
AAPD-220 W	65.2 ± 1.4	55.9 ± 0.5	28.6 ± 0.2	9.2 ± 0.3	6.3 ± 0.5
Reference values		C%	O%	Si%	N%
APTES monomer		64.3	21.4	7.1	7.1
APTES polymer (theoretically/obtained by Lecoq *et al.*[12])		46.2/52	23.1/21	15.4/14	15.4/13

The WCA measurements clearly show that the plasma polymerization results in a significant increase in wettability in comparison to UHMWPE. As expected, the bare substrate is hydrophobic, which originates from the absence of polar groups in UHMWPE. This is also confirmed by the XPS atomic composition, as a non-significant number of O-atoms were measured. The various AAPD-APTES coatings have similar average WCA values, ranging from 62° to 66°. Therefore, plasma power does not have a very significant influence on the wettability of the resulting films within the employed power range. The standard deviations are below 2°, indicating that the PlasmaSpot® system is capable of depositing homogeneous APTES-based coatings. The XPS atomic composition, as presented in **Table 2**, is very similar for the AAPD-APTES layers deposited at different applied powers, which is in line with the similar wettability obtained for the three conditions. The resulting coatings contain the elements which are expected based on the monomer structure. The high C-content illustrates that the AAPD-APTES films are highly organic in nature, which was already observed for AAPD and PECVD of APTES before.[16, 29] High-resolution XPS spectra are displayed in **Figure 3** for a more detailed analysis of the surface chemistry. It should be noted that 4 different spectra obtained on one sample were very similar. Therefore, only one XPS spectrum is shown per condition in this paper.

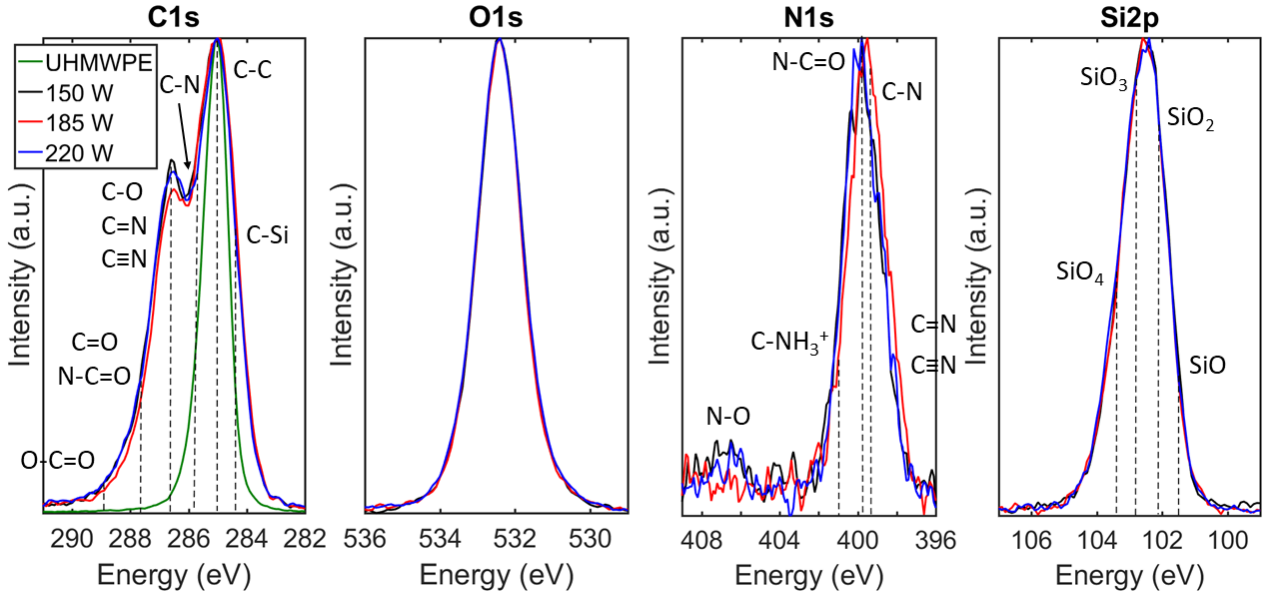

Figure 3. High-resolution XPS spectra for UHMPWE and AAPD-APTES coatings deposited at different powers.

Figure 3 clearly shows that the AAPD-APTES coatings deposited at different powers have very similar high-resolution XPS spectra, while the UHMWPE only has a single contribution at 285 eV for C-C and C-H bonds, as expected. The broadness of the N1s spectra suggests that a variety of N-containing functionalities are present. Designating the exact nitrogen-containing functional groups is very difficult because of the ambiguity in peak energy locations, as also highlighted in section 2.5. It seems likely that unsaturated (like imines, and/or (iso)nitriles), oxidized (amides and/or other functionalities such as imides, as highlighted by Truica-Marasescu *et al.*), and charged functionalities (protonated primary

and secondary amines) can be present in the main peak centered around 399.5 - 399.8 eV.[33] Furthermore, a small contribution of N-O bonds is also observed. The formation of these different chemical groups is certainly the result of plasma-precursor/coating interactions and/or post-plasma oxidation, which are well-known phenomena for different amine-based precursors. All these processes result in the formation of a variety of N-containing functionalities.[12, 16, 21, 33] The difference in the main peak in the C1s spectra between the UHMWPE substrate and the AAPD coatings is clearly in line with the expected chemistry, as contribution for C-Si, C-C and C-N can be distinguished. The contribution around 286.6 eV can be mainly attributed to C-O bonds, although contributions of C=N and C≡N bonds are present at similar energies.[12] C=N-containing functionalities, such as imines, can be present, but their contribution will be low based on the N1s peak shape and N-content. (Iso)nitriles should not be considered, as their presence was not confirmed by FTIR, which will be discussed in the next section. By comparing the coatings deposited in this study to previously reported APTES-based plasma polymer coatings, additional insights can be obtained in the nature of the C-O bonds.[12, 20, 29] This comparison (see Supplementary data) highlights that the C-O bonds in the AAPD-APTES coatings mainly originate from the preservation of the monomer structure (Si-O-C bond). Definitely, the aforementioned in- and/or post-plasma oxidation can also contribute to a certain extent to this observed peak. The C1s spectra also show a significant contribution of C=O and/or N-C=O bonds, while a small contribution of O-C=O can also be observed. These oxygenated groups are most likely formed by in- or post-plasma oxidation, as suggested by Rao *et al*., for example and proposals of the involved chemical pathways can be found elsewhere.[12, 19, 34-35] The occurrence of plasma-induced oxidation, either in- or post-plasma, is also supported by the higher amount of O-atoms in the coating as compared to the theoretically expected values of the monomer, which are shown in **Table 2**. The O1s spectra, with the center of the peaks located at 532.4 eV, are challenging to analyze because of the absence of reference studies, as highlighted before.[2] The peak location of the Si2p spectra is close to the energy associated with the expected oxidation state (SiO_3) of APTES, namely 102.8 eV, but the broadness illustrates that the silicon atoms are also attached to different numbers of O-atoms. This illustrates that the interaction of the plasma with the APTES molecules results in scission of the Si-O and/or Si-C bonds. The presence of partial monomer fragmentation during the deposition process is also supported by the difference in N-content and Si-content, as the amount of N- and Si-atoms is equal in the APTES molecule. On the other hand, the presence of a significant amount of Si-O-C bonds indicates that the plasma fragmentation is less significant than in the case of PECVD of APTES-based coatings (see supporting information). This is in line with the differences in the process, as PECVD uses monomer molecules in the vapor phase, allowing plasma-precursor interactions with every monomer molecule. In contrast, for AAPD, the monomer is introduced in small aerosol droplets, which can shield a number of molecules from the plasma. A similar observation was made by Nisol *et al*., who observed a better retention of the tetraglyme precursor in AAPD than in PECVD at the same power input.[36] The presence of a limited monomer fragmentation is also supported by the atomic composition of the AAPD-APTES coatings, which is more similar to the composition of the monomer than of the conventionally polymerized APTES, as expected theoretically or obtained experimentally (see **Table 2**, deviations on the atomic composition of the synthesized and theoretical APTES-based polymers can be caused by an incomplete reaction of the incorporated molecules).[20] This suggests that conventional hydrolysis of the Si-O-C-bonds and subsequent condensation of silanols, which is the typical polymerization mechanism, is not dominant. A significant amount of Si-O-C-bonds appears to be preserved in the coating and plasma-induced oxidation results in the formation of a variety of functionalities.

As such, the AAPD-APTES coatings have a complex organosilicon-based chemistry containing a variety of polar functional groups. The introduction of these groups is in line with the observed decrease in WCA as compared to the untreated UHMWPE, because the wettability of a surface depends on both the surface chemistry and morphology.[37] As the AFM measurements indicated that the samples only became slightly rougher after the AAPD-APTES process, the increased wettability can be mainly attributed to the change in surface chemistry.

3.1.3. ATR-FTIR

The infrared spectra obtained for the uncoated UHMWPE substrate and as-deposited AAPD-APTES coatings acquired for three powers are depicted in **Figure 4**. It should be noted that the 9 spectra that were collected from three samples are very similar, indicating that the AAPD-APTES coatings are deposited in a reproducible and homogeneous way on the UHMWPE substrate. Therefore, only one spectrum is shown per condition. The reader is referred to another study if there is a wish to compare the spectra of the different coatings to the spectrum of the APTES monomer.[29]

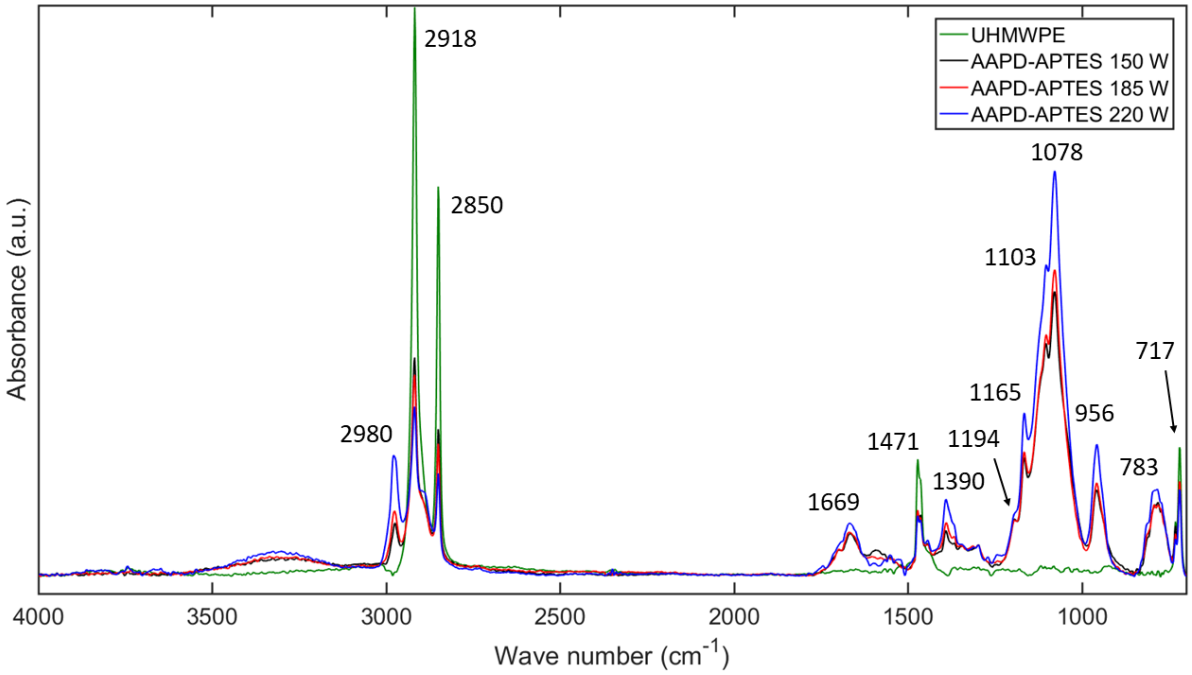

Figure 4. ATR-FTIR spectra for uncoated UHMWPE and as-deposited AAPD-APTES samples with different plasma input powers.

Figure 4 clearly shows that several new peaks are superimposed on the original FTIR spectrum of the substrate. The variation in power does not lead to different peaks in the spectra, indicating that no new detectable functionalities are formed by changing this parameter. **Table 3** summarizes the assignment of the different peaks.

Table 3.FTIR peak assignment for uncoated UHMWPE and the AAPD-APTES coatings.

Origin	Wavenumber (cm^{-1})	Peak assignment
Substrate and AAPD-APTES coating	2918, 2850	C-H stretching in $-CH_2-$.[38-39]
	1471	C-H deformation.[38-39]
	717	C-C rocking.[38-39]
AAPD-APTES coating	3500-3000	OH stretching in alcohol and/or silanol.[16, 39] N-H stretching in amine and/or amide. [16, 39]
	2980	C-H stretching in $-CH_3$.[39]

	1750-1630	1666 cm^{-1}: C=O stretching in amides.[3, 16] shoulder 1690-1750 cm^{-1}: ketones/aldehydes, carboxylic acids and/or esters.[16, 39] additional contribution of C=N stretching in imines can be expected.[16, 39]
	1630-1500	amide II band and/or N-H deformation in secondary amines.[15, 39]
	1500-1250	Various vibrations from CH_3, Si-CH_2, C-N and O-H, among others.[12, 16]
	1200-1000	Variety of vibrations relating to Si-O-C stretching and Si-O-Si stretching.[12, 16] Peak at 1165 cm^{-1} can be attributed to C-H rocking in Si-O-CH_2-$\underline{CH_3}$.[16, 40]
	956	CH_3 rocking in Si-O-CH_2-$\underline{CH_3}$ and possibly, Si-O-C stretching.[39-40]
	783	Vibration of the full CH_3CH_2O-group in Si-O-CH_2-CH_3.[16, 40]

Table 3 shows that the different AAPD-APTES coatings are composed of a variety of chemical functionalities. In general, some peaks can be related to the preservation of the monomer structure, such as the contributions at 956 cm^{-1}, 783 cm^{-1}, the Si-O-C stretching and C-H rocking in between 1200-1000 cm^{-1} and the different vibrations of the N-H bond. Most other peaks are related to plasma-induced functional groups. Mainly the contributions between 3500-3000 cm^{-1} and 1750-1630 cm^{-1} are worth mentioning. These peaks indicate the presence of a variety of functionalities that are formed due to different oxidation processes during the plasma polymerization. The presence of these peaks suggests that alcohols, amides, ketones/aldehydes and/or carboxylic acids/esters can be found throughout the coating. This suggests that their formation mainly occurs during the deposition process, as ATR-FTIR probes also the bulk of the coatings.[41] Nevertheless, the contribution of post-plasma oxidation cannot be excluded as well. The presence of Si-O-Si-related peaks indicates that some APTES molecules underwent a reaction similar to conventional polymerization, which can either result from contact with humid air in the precursor container and/or in the afterglow, or from plasma-induced coupling reactions. Between 1669 and 2850 cm^{-1}, no absorbance is observed, which indicates that there is no detectable contribution of C≡N and C≡C. As such, the presence of nitriles and isonitriles in the coating can be neglected and the broadness of the N1s peaks can be attributed to the presence of C=N bonds. These bonds are typically observed in N-containing plasma polymers and can lead to an additional contribution between 1630 cm^{-1} and 1690 cm^{-1}, among others.[20, 39]

It can be concluded that the FTIR and XPS measurements of the AAPD-APTES coatings correspond well. They both indicate that the plasma polymers contain a variety of functionalities. The monomer structure is retained to a certain extent and the plasma power does not have a significant effect on the coating's chemistry within the employed parameter range. This observation is not in line with the generally accepted concept for PECVD that the energy applied per molecule, which can be varied by changing plasma power and monomer flow, directly influences the surface chemistry.[42] A similar observation was made for the AAPD of PEG-like coatings.[6, 36] However, more data would be needed to confirm the influence of plasma power and atomizing flow, as Da Ponte *et al.*, for example, observed some effect of the plasma power on the surface chemistry of AAPD-based PEG-like coatings.[43]

3.2. Comparison of the physicochemical properties of AAPD-APTES and ppHMDSO-APTES coatings

In this section, the physicochemical properties of the AAPD-APTES coatings obtained at 150, 185 and 220 W are compared to the ppHMDSO-APTES coatings, for which the deposition was already optimized in a previous study.[2] The surface wettability, morphology and chemistry were compared by using WCA, AFM and XPS measurements, respectively. ATR-FTIR was not employed to make the comparison between the coatings, as the APTES layer on top of the ppHMDSO coating was too thin to measure a significant ATR-FTIR-signal. **Table 4** summarizes the WCAs and atomic composition of the coatings obtained after the different steps used to synthesize the ppHMDSO-APTES coatings.

Table 4. WCAs and XPS atomic composition for ppHMDSO, air plasma-activated ppHMDSO (Apa-ppHMDSO) and ppHMDSO-APTES coatings.

	WCA (°)	XPS atomic composition			
		C%	O%	Si%	N%
ppHMDSO	105.3 ± 0.8	47.6 ± 0.5	28.8 ± 0.1	23.5 ± 0.6	
Apa-ppHMDSO	4.5 ± 2.3	26.4 ± 2.1	50.9 ± 2.3	22.6 ± 0.3	
ppHMDSO-APTES	56.5 ± 2.1	53.0 ± 1.6	26.0 ± 0.8	12.0 ± 1.3	9.1 ± 0.4

The wettability and surface chemistry of the ppHMDSO coating, as presented in **Table 4**, clearly indicate that the UHMWPE substrate is successfully coated with a PDMS-like HMDSO-based plasma polymer film. Indeed, the UHMWPE substrate's wettability is slightly lower than the ppHMDSO coating's wettability and the XPS atomic composition clearly indicates the formation of an organosilicon layer on the surface. The wettability is very similar for this coating in comparison to the ppHMDSO layer obtained in a previous study, in which a different medium pressure plasma polymerization reactor was used.[2] The atomic composition is slightly different, as the here-presented coating is slightly more oxidized, which can be caused by a higher residual air content in the reactor, or by a higher monomer fragmentation.[44-45] The subsequent air plasma activation step results in the formation of a very hydrophilic layer, which can be explained by the introduction of oxygen atoms into the surface, as observed in the XPS atomic composition. This trend is very similar to the one observed in a previous study, although this plasma step used a different power and treatment time.[2] This plasma activation step is necessary to introduce silanol groups onto the surface with which APTES, or other silanization agents, can react to form a stable layer, as comprehensively studied before.[2] The subsequent APTES-functionalization reaction results in the formation of a N-containing organosilicon surface layer that is very similar to the coating obtained in a previous study.[2] This clearly demonstrates the versatility of the employed approach based on silanization and HMDSO plasma polymerization, as a comparable APTES-based coating chemistry can be obtained with different plasma set-ups and/or parameters. The APTES silanization also leads to a significant increase in the WCA as compared to the Apa-ppHMDSO coatings. The standard deviation of the WCAs obtained on the ppHMDSO-APTES coatings is relatively low, illustrating that this process is capable of depositing homogeneous and reproducible films. The wettability of these coatings is slightly lower than that of APTES-modified Si substrates, for which WCA values of approximately 50° were reported.[46] However, a large difference in wettability is observed between APTES-based self-assembled monolayers (SAMs).[47-49] It was suggested that this difference originates from the different orientation of the amine functionality.[49]

As mentioned before, the surface wettability depends on the surface morphology and chemistry, which are discussed in the following sections.[37] **Figure 5.A**. shows that the morphology of the ppHMDSO-ATPES coating is very similar to the UHMWPE morphology that is shown in **Figure 2.A.,** although some sharp features with heights in the range of 100 - 400 nm seem to be introduced onto the surface. This also results in the increase in R_q value from 166.9 ± 74.5 nm to 286.9 ± 43.6 nm after coating deposition. These features were also observed before on the ppHMDSO-APTES coating

deposited on glass and other APTES-based layers on glass and silica under certain conditions. It can be either dust particles or fragments formed in the reaction mixture because of water impurities that can subsequently get incorporated in the coating.[2, 47, 50]

The XPS atomic composition of the ppHMDSO-APTES film, as presented in **Table 4**, is relatively similar to the composition of the AAPD-APTES coatings, although the C- and O-content is slightly lower for the former coatings, while the Si- and N- content is slightly higher. The atomic composition of the ppHMDSO-APTES coating shows that the Si- and N-content are significantly different, which indicates that the APTES layer is thinner than the XPS analysis depth (approximately 5 to 10 nm) and that part of the underlying Apa-ppHMDSO coating with a higher Si-content is still measured.[51-52] This is in line with multiple studies that have assessed the thickness of APTES layers on Si wafers by ellipsometry.[47, 53] Additionally, it is also in line with previous work on these ppHMDSO-APTES coatings, that showed that under the here-employed conditions, a ppHMDSO underlayer with a thickness of around 50 nm is deposited, after which the thin APTES-based layer is added.[25] Before further analysis, high-resolution XPS spectra of the ppHMDSO-APTES coating will be overlapped with the spectra of the AAPD-APTES coatings to allow a complete surface chemistry comparison. **Figure 5**.**B.** shows this comparison. For a detailed analysis of the high-resolution XPS spectra of ppHMDSO, Apa-ppHMDSO and ppHMDSO-APTES coatings, the reader is referred to a previous study.[2] Here, the focus will be on the differences in between the AAPD- and ppHMDSO-APTES coatings.

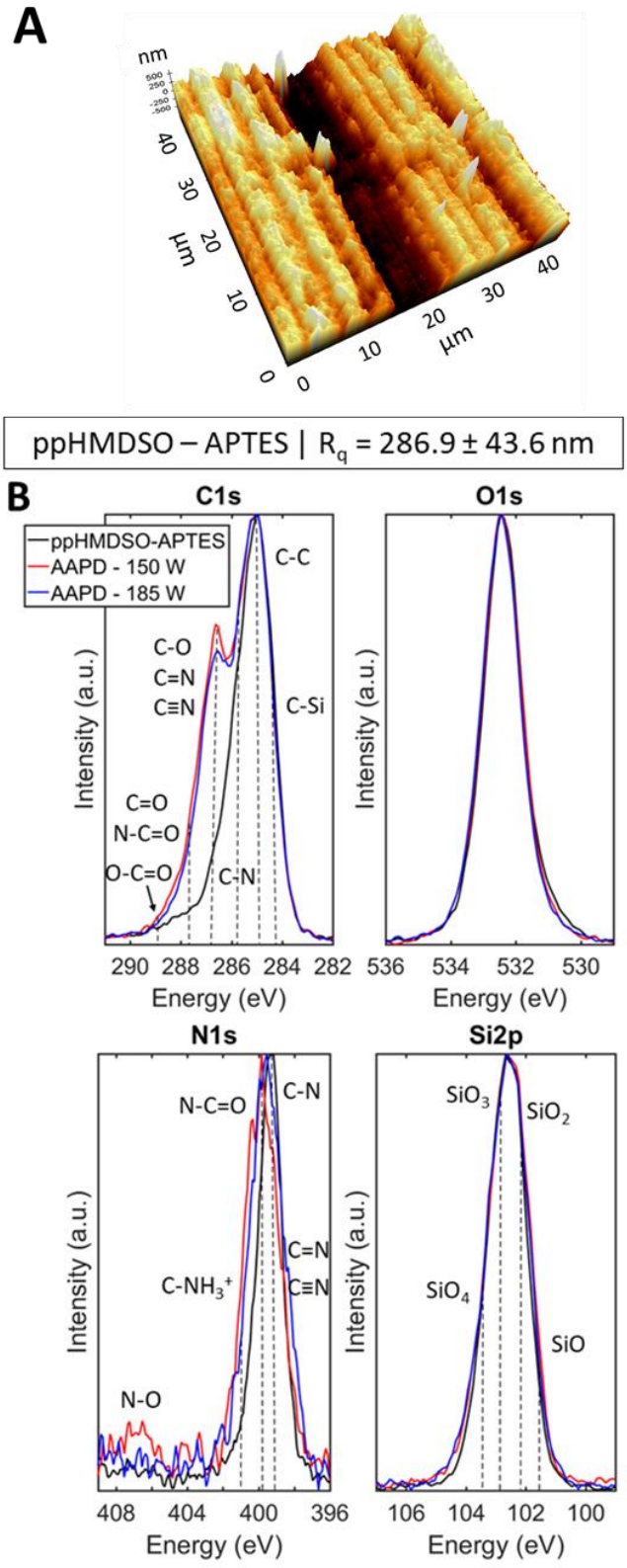

Figure 5. AFM image of the morphology and R_q value of the ppHMDSO-APTES coating on UHMWPE (A) and high-resolution XPS spectra of the ppHMDSO-APTES coating and AAPD-APTES coatings deposited at 150 and 185 W (B).

Figure 5.B. clearly shows that the surface chemistry of the ppHMDSO-APTES coatings is significantly different from the AAPD-APTES coatings, despite the similarities in the XPS atomic composition. This could also explain the slight difference in wettability between the two different deposition processes,

as can be observed by comparing **Table 2** and **Table 4**. The O1s spectra, with peaks centered at 532.4 eV, and the Si2p spectra, with peaks centered at 102.6 eV, show only minimal differences and are therefore not discussed in more detail. For the C1s curve, the contributions around 286.6 eV (C-O, C=N, C≡N) and 287.7 eV (C=O, N-C=O) are significantly lower for the ppHMDSO-APTES coating than for the AAPD-APTES coatings, while the contribution of O-C=O is completely absent for the former layer type. For the ppHMDSO-APTES coatings, the presence of C-O (C=N and C≡N can be neglected, in this case) bonds can be explained by a residual amount of unreacted Si-O-C bonds in the APTES-based layer that is deposited. The N-C=O/C=O bonds could be the result of oxidation of the amine functionality in the reaction mixture or because of interactions with ambient air after removal of the sample and before vacuum incubation.[11] For the AAPD-APTES coatings, these oxidized functionalities are originating from aforementioned plasma-induced modifications by fragmentation. The N1s spectra also show differences, as the ppHMDSO-APTES coating has a narrower peak than the different AAPD-APTES coatings. This peak has a maximum at 399.3 eV and a small contribution at 400.9 eV ($C\text{-}NH_3^+$). This clearly indicates that the N-atoms are mostly incorporated in this coating as (protonated) primary amines, as discussed in detail before and as expected based on the employed reaction.[2] The protonated amines can be the result of the presence of a minimal amount of water in the reaction mixture, or because of interaction with water vapor in the ambient air after removal of the sample and before vacuum incubation. A very small contribution of amides could be present as well, which is additionally supported by the small contribution at 287.7 eV in the C1s spectrum. For the AAPD-APTES spectra, the broader N1s spectra indicate the presence of a variety of N-containing functionalities, as discussed in section 3.1.2.

These XPS measurements allow the conclusion that the ppHMDSO- and AAPD-APTES coatings have a completely different surface chemistry. The ppHMDSO-APTES coatings are composed of a PDMS-like plasma polymer bottom layer covered by a APTES-based layer that is similar to conventionally polymerized APTES, although the presence of C-O suggests that not all molecules are completely polymerized. On the other hand, the AAPD-APTES coatings seem to be composed of cross-linked APTES molecules that underwent conventional polymerization to a limited extent, while plasma-induced oxidation and fragmentation contributes significantly to the coating chemistry. The differences in the C1s and N1s spectra clearly show the superior chemical selectivity of the ppHMDSO-APTES coatings, which was hypothesized before.[2] This illustrates that the silanization-based approach is capable of depositing coatings with a selective functionality that surpasses any other APTES-based plasma polymer film. On the other hand, the drawback of this approach is that it requires a multi-step process that contains one wet-chemical step.

3.3. Comparison of aging behavior of AAPD-APTES and ppHMDSO-APTES coatings

3.3.1. WCA and XPS

WCA measurements were performed to assess the aging of the different coatings. Different aging processes, such as post-plasma oxidation of dangling bonds and rearrangement of near surface chemical groups (hydrophobic recovery), may result in a change in wettability.[11, 54] **Figure 6** shows the evolution of wettability for the AAPD- and ppHMDSO-APTES coatings for a period of 15 days during storage in ambient air at room temperature.

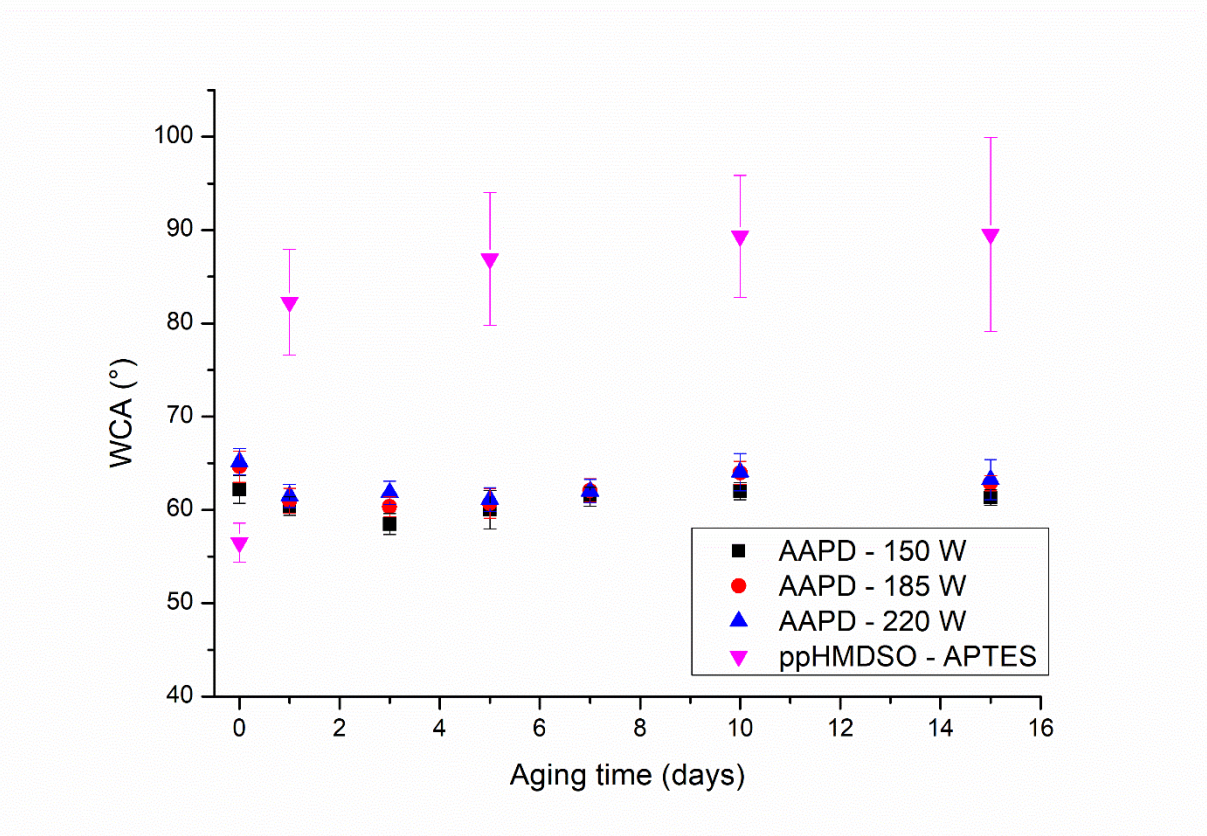

Figure 6. WCA values as a function of aging time for the AAPD-APTES coatings deposited at 150, 185 and 220 W and the ppHMDSO-APTES coating.

From **Figure 6**, it becomes clear that the AAPD-APTES coatings deposited at different powers show a very similar wettability aging behavior. The WCA values obtained on the coatings for 1, 3 and 5 days are slightly lower than the values obtained directly after the deposition. For 7 and 10 days of aging, a slight increase in the WCA values is observed again, after which the wettability remains similar until 15 days of aging. However, the differences appear to be very small. This is in contrast with the trend in wettability for the ppHMDSO-APTES coatings as a function of aging time. A significant decrease in wettability is observed for these coatings, as the average WCA value increases from approximately 57° to approximately 82° after just one day of aging. For longer storage times, the average WCA value still increases a little bit, as observed for 5, 10 and 15 days, although the standard deviations are relatively high. It can also be observed that these standard deviations are significantly higher for the ppHMDSO-APTES coatings than for the AAPD-APTES coatings, despite the low standard deviation for the former coating directly after deposition. This relatively high standard deviation values are the result of a limited reproducibility and homogeneity, as deviations can be observed both on one sample and between different samples. To obtain a better understanding of the chemical processes that could relate to these wettability changes, XPS measurements were conducted for 1, 5 and 10 days of aging, as no additional effect in the wettability was observed for 15 days of aging. **Table 5** summarizes the atomic composition as determined by XPS as a function of storage time for the 4 different APTES-based coatings.

Table 5. XPS atomic composition as a function of storage time for the ppHMDSO-APTES and AAPD-APTES coatings deposited at 150, 185 and 220 W.

	ppHMDSO-APTES				AAPD-APTES 150 W			
	C%	O%	Si%	N%	C%	O%	Si%	N%
0 days	53.0 ± 1.6	26.0 ± 0.8	12.0 ± 1.3	9.1 ± 0.4	55.4 ± 0.4	28.7 ± 0.6	9.4 ± 0.3	6.5 ± 0.4
1 day	52.9 ± 3.0	27.2 ± 2.7	11.7 ± 1.3	8.2 ± 1.2	50.8 ± 0.5	31.7 ± 0.3	10.8 ± 0.3	6.7 ± 0.2
5 days	51.2 ± 3.0	30.7 ± 2.0	12.3 ± 1.3	5.8 ± 0.4	49.1 ± 0.5	33.4 ± 0.1	11.3 ± 0.5	6.2 ± 0.1
10 days	50.9 ± 0.3	30.9 ± 0.4	11.0 ± 0.3	7.2 ± 0.1	48.1 ± 0.4	33.6 ± 0.2	11.9 ± 0.2	6.4 ± 0.4
	AAPD-APTES 185 W				AAPD-APTES 220 W			
	C%	O%	Si%	N%	C%	O%	Si%	N%
0 days	56.1 ± 0.5	28.2 ± 0.4	9.5 ± 0.4	6.3 ± 0.5	55.9 ± 0.5	28.6 ± 0.2	9.2 ± 0.3	6.3 ± 0.5
1 day	50.8 ± 0.8	32.0 ± 0.6	10.5 ± 0.3	6.6 ± 0.9	53.7 ± 0.3	30.9 ± 0.3	9.4 ± 0.2	6.0 ± 0.4
5 days	49.1 ± 0.4	32.7 ± 0.6	11.0 ± 0.2	7.2 ± 0.3	50.6 ± 0.4	33.1 ± 0.6	10.2 ± 0.5	6.1 ± 0.2
10 days	48.0 ± 0.5	34.1 ± 0.7	11.4 ± 0.1	6.4 ± 0.2	48.8 ± 0.9	33.8 ± 0.5	10.8 ± 0.3	6.7 ± 0.7

Table 5 clearly illustrates that all the different coatings are prone to an aging effect. For the ppHMDSO-APTES coating, a slight decrease in C- and N-content and an increase in O-content is observed. The measurements for 1 and 5 days are indicating a decreasing trend, although the standard deviations for these samples were higher. The decrease in N-content seems to be also significant. However, variations in N-content between 6 and 10% were observed before as well for non-aged ppHMDSO-APTES samples.[2] As such, it can be concluded that the aging of the ppHMDSO-APTES coating over 10 days results in a significant increase in O-content at the expense of a slight decrease in C- and N-content, while the Si-content stays more or less constant. The most significant aging occurs in the first 5 days, as the atomic content only changes minimally between 5 and 10 days of aging. The AAPD-APTES coatings show a different behavior as the C-content decreases significantly, while the O- and Si-content increases. In contrast, the N-content stays the same over the complete aging period. These coatings are also more homogeneous than the ppHMDSO-APTES coating. Moreover, it can be observed that the aging behavior is very similar for the three different applied powers, as very comparable atomic compositions are obtained for all the different aging days. The most significant aging occurs within the first 5 days for the three different powers, as the atomic content only changes minimally between 5 and 10 days of aging. As studies on the aging behavior of plasma polymerized APTES coatings are limited, an aging study on the PECVD of APTMS, as an alternative aminosilane, can be used for a comparison. Borris *et al*. observed a different aging behavior for these plasma polymers. They used different carrier gases and observed an O-increase of only 2 % after 28 days of aging for coatings deposited in N_2 and Ar, while the C-content remained similar and the Si-content decreased accordingly. For coatings deposited in He, a more significant increase in O-content of 5 % was observed, but the C-content remained similar for this coating, as well. As such, it appears that aminosilane-based plasma polymers with different atomic compositions can have a very different aging behavior. To get a better understanding of the involved processes, the high-resolution XPS spectra, which are shown in **Figure 7**, are studied, as well.

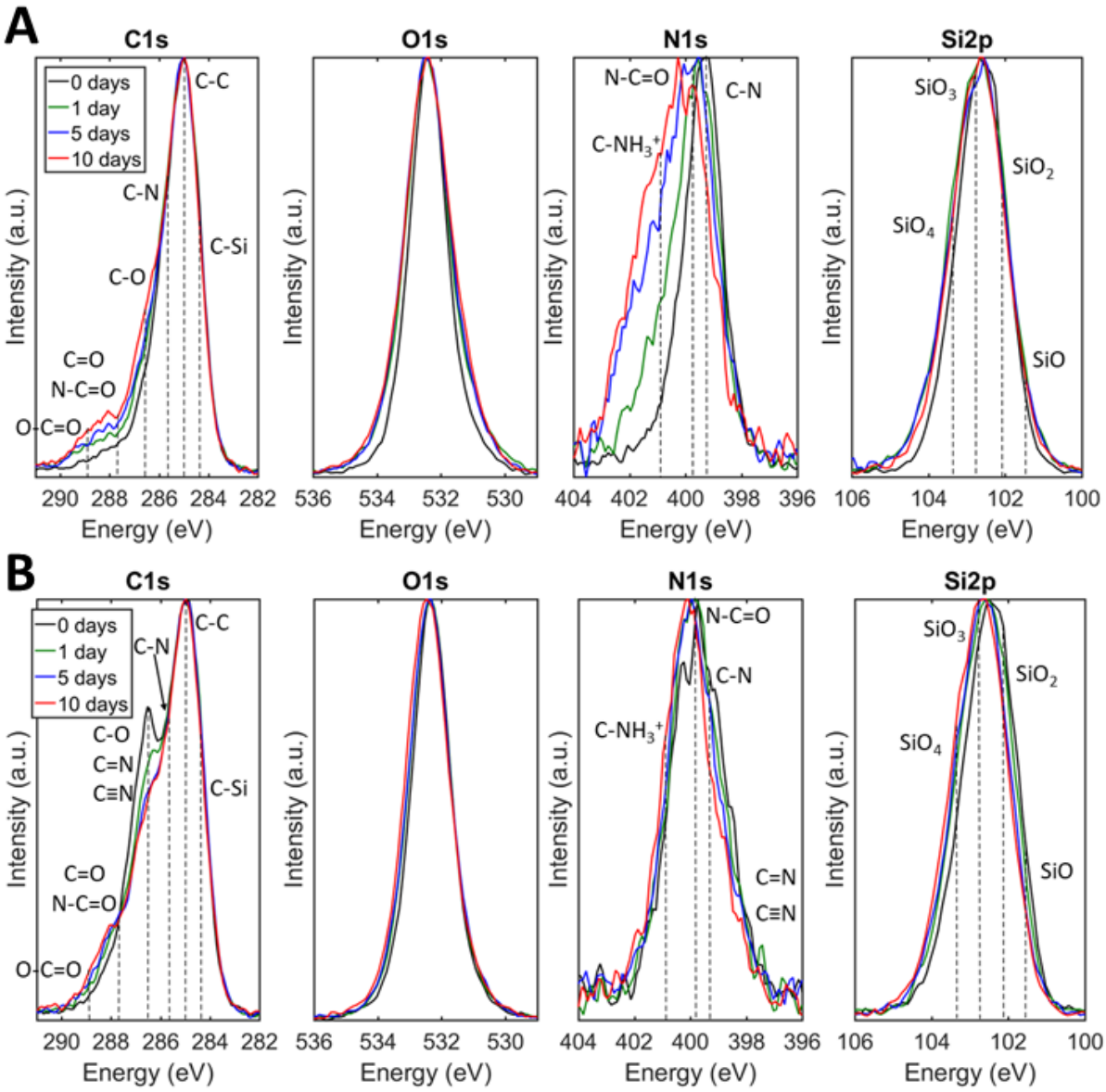

Figure 7. High-resolution XPS spectra for ppHMDSO-APTES (A) and AAPD-APTES deposited at 150 W (B) for different days of aging.

For the AAPD-APTES coatings, the high-resolution XPS spectra showed a very similar behavior for the different measurement points and different powers. Therefore, only the spectra of the coatings deposited at 150 W are shown in **Figure 7**.**B**, while the spectra for the coatings deposited at other powers can be found in the Supplementary data (Figure S2). The high-resolution XPS spectra of the AAPD- and ppHMDSO-APTES coating for different aging days clearly illustrate that the surface chemistry of both films is changing upon contact with ambient air. For both coating types, the peak of the Si2p curve remains close to the energy expected for the most prevalent Si oxidation state (SiO_3), although it is difficult to assign the peak broadening to an occurring chemical aging process. For the O1s spectra, relatively small changes are present, which could relate to the formation of amides (typically located around 531–531.5 eV), Si-O-C hydrolysis and/or silanol condensation, but further analysis is challenging because of the aforementioned absence of confirmatory reference studies.[2] For the C1s and N1s peaks, it is possible to assign the changes to multiple aging processes.

Table *6* summarizes these different processes for both coatings. The contribution of N-O bonds is not shown to clearly display the differences between the spectra, as **Figure 3** clearly indicated that this contribution is low. Moreover, for the aged samples, no contribution was observed anymore.

Table 6. Aging processes of the ppHMDSO- and AAPD-APTES coatings and their relation to the changes in the XPS measurements.

Aging process	ppHMDSO-APTES coating	AAPD-APTES coatings
Protonation of primary and/ or secondary amines	Significant protonation of primary amines, evidenced by the shift in N1s. The increased contribution around 286.6 eV could relate to the formation of C-NH_3^+, as it can be expected that the protonation will result in a shift towards higher binding energies for primary amines, which can be typically found around 285.7 eV.[28] For now, there is no further experimental data to confirm this hypothesis. Carbonates can be the side-product of this reaction, which can explain the increase in O-C=O contribution and O-content.[55]	Occurring to a more limited extent, in comparison to the ppHMDSO-APTES coating, as evidenced by the more limited shift in N1s.
Oxidation	Primary amines are known to oxidize by exposure to ambient air.[56] The increased contribution of N-C=O suggests the presence of this aging process, as amides and carbamates can be formed upon exposure to O_2 and CO_2, respectively.[55-56] N-C=O formation is also in line with the shift in the N1s peak.[28] This also relates to the increase in O-content.	A distinction can be made between (1) plasma-induced oxidation and (2) primary amine oxidation as described for the ppHMDSO-APTES coating. Both processes relate to the increase in O-content: 1: Plasma-induced oxidation can explain increased contributions of C=O, N-C=O and O-C=O in the C1s spectra. N-C=O can be formed via oxidation of α-amino methylene radicals that are created by plasma-precursor interactions.[35] Formation of this group is in line with the shift in the N1s curve. C=O and O-C=O can be formed via a similar oxidation of C-centered radicals.[11] 2: Primary amine oxidation can explain the shift in the N1s curve, but can be expected to be less important, as the amount of primary amines is low. This is indicated by the absence of a significant protonation and the difference in N1s between ppHMDSO- and AAPD-APTES coatings.
Hydrolysis	No indication of this process.	1: Hydrolysis of Si-O-C bonds: evidenced by the decreased contribution of C-O bonds (C=N and C≡N bonds can be considered as less prevalent, based on ATR-FTIR and XPS N1s spectra). 2: Hydrolysis of imines: the formation of amines and ketones/aldehydes could be in line with the small changes in the N1s spectra and with the C=O formation and C=N decrease in the C1s

		spectra, respectively. It is, however, quite difficult to predict the kinetics of this reaction.[11]

The different occurring aging mechanisms mentioned in
Table *6* are all the result of the interaction between the coatings and humid air. For the ppHMDSO-APTES coating, protonation appears to be more prevalent than oxidation. This is evidenced by the significant change in the N1s spectra, as protonated amines are typically observed at higher energies than amides.[28] The changes in the C1s and N1s spectra appear to be in line with the trend in atomic composition, as most of the changes to the XPS measurements occur in the first 5 days. It should be noted that protonation and carbamate formation, as one of the oxidation processes, are both reversible, thus allowing a (partial) recuperation of the high primary amine content after 15 days of aging in air by exposure to certain media (basic aqueous media or environment without CO_2). In general, the aging behavior of the ppHMDSO-APTES coating resembles the aging of APTES layers on conventional substrates. This indicates that the changes in the surface chemistry are mostly related to changes in the APTES-based top layer of the coating. Recently, it was shown that the Apa-ppHMDSO layer is also prone to a significant aging effect, but it appears to not influence the aging of the resulting ppHMDSO-APTES layer.[25] Most changes to the high-resolution XPS spectra occur in the first five days, which is in line with the observations for the XPS atomic composition, as presented in **Table 5**. For the AAPD-APTES coatings, oxidation and hydrolysis seem to be more important than the protonation of primary and/or secondary amines. This additionally supports the observation that the amount of primary amines in this coating is significantly lower than in the ppHMDSO-APTES coating, resulting in a more limited change in the N1s spectra. Most of the changes in the high-resolution XPS spectra are occurring in the first 5 days of aging, which is also in line with the trends in atomic composition. This confirms that the formation of ketones/aldehydes, amides, carboxylic acids and/or esters due to oxidation is the main reason for the increase in O-content.

As such, it can be concluded from WCA and XPS measurements that the ppHMDSO- and AAPD-APTES coatings are prone to aging and have a different aging behavior, although oxidation was involved for both films. The fact that the amount and chemistry of polar functionalities on the ppHMDSO-APTES coatings did not significantly reduce, while the average WCA values significantly increased, can be explained by the different analysis depth of both techniques. Indeed, the analysis depth of WCA measurements is even lower than of XPS.[57] The observed measurements suggest that the hydrophilic functionalities, namely amines and aging products like amides and protonated amines, re-orientate away from the surface, which results in a lower hydrophilicity for the aged ppHMDSO-APTES coatings. This behavior is similar to the aging of plasma activated polymer substrates.[58] For the AAPD-APTES coatings, the average WCA values remain similar, which could suggest that the cross-linked nature of the plasma polymer film does not allow a similar reorientation as observed for the ppHMDSO-APTES coatings. As such, it appears that the different chemical processes like oxidation, hydrolysis and/or protonation do not result in significant changes in the coatings' wettability.

3.3.2. ATR-FTIR

Besides XPS, also ATR-FTIR spectra have been acquired for the AAPD-APTES coatings deposited at different applied powers after 1, 5, and 10 days of aging. The spectra upon aging show very similar changes for all plasma powers. Therefore, only the results for 150 W are presented in **Figure 8**. The ATR-FTIR spectra for the aged AAPD-APTES coatings deposited at 185 W and 220 W are shown in Figure S3 in the Supplementary data. As mentioned before, ATR-FTIR was not employed to study the aging of the ppHMDSO-APTES coating, as the APTES layer on top of the ppHMDSO coating was too thin to measure a significant ATR-FTIR-signal.

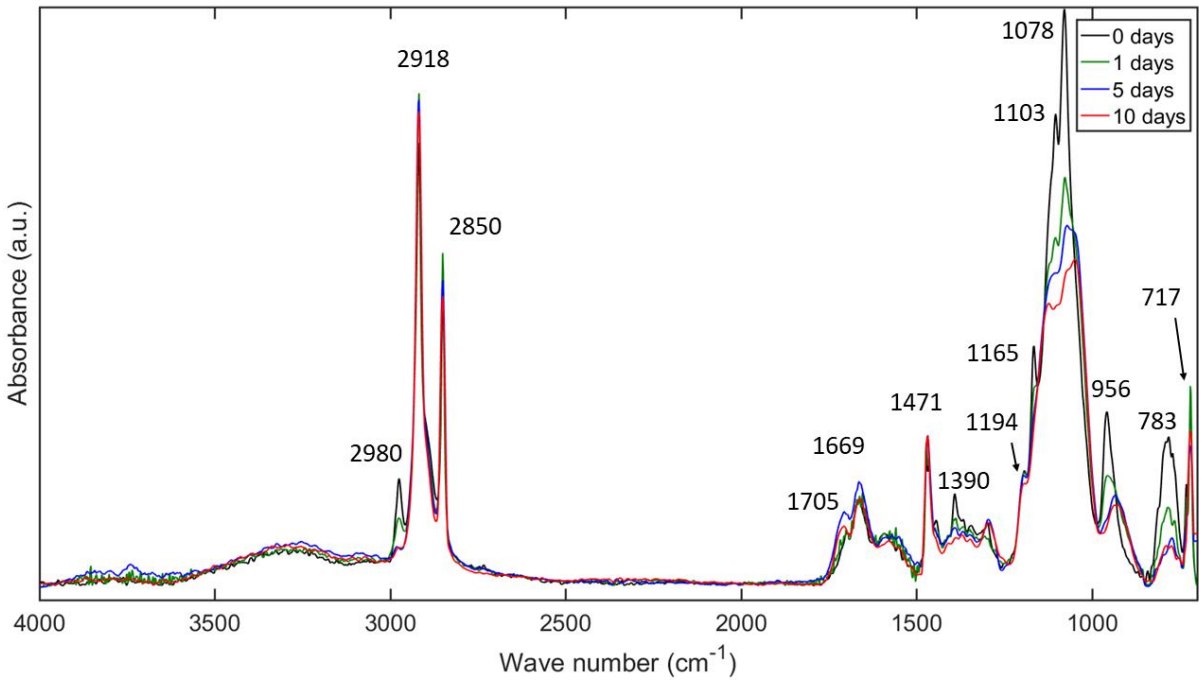

Figure 8. ATR-FTIR spectra of AAPD-APTES coatings deposited at 150 W directly after deposition and after aging for 1, 5, and 10 days.

The most significant changes in the ATR-FTIR spectra upon aging are observed for the peaks at 783 cm^{-1} and 956 cm^{-1} and between 980-1200 cm^{-1}. A small change can also be observed between 1630-1750 cm^{-1}, which is most pronounced at higher wavenumbers. This relates to the increasing amount of ketones/aldehydes, carboxylic acids and/or esters upon aging (see **Table 3**), which results from post-plasma oxidation, as also observed in the XPS measurements. The limited change in the FTIR spectra suggests that this process is, however, mainly occurring at the surface. The other changes in the FTIR spectra all relate to the hydrolysis of Si-O-C-bonds in humid air.[20, 59] **Table 3** indicates that the significant decrease of the peaks at 783 cm^{-1} and 956 cm^{-1} relates to different vibrations of the CH_3CH_2-O-Si-structure. The shoulder of the latter peak that is formed upon aging is related to contributions of Si-OH stretching (around 930 cm^{-1}) and ethanol skeletal vibration (around 882 cm^{-1}), which are the result of the breakage of the Si-O-C bond.[39-40] This also seems to induce a higher contribution of C-H stretching in $-CH_3$ at 2980 cm^{-1}. These changes can thus be related to the disappearance of the Si-O-CH_2-CH_3 structure, the formation of ethanol, and the self-condensation of silanol groups that are formed due to hydrolysis, as discussed in detail before by Peña-Alonso *et al*. for conventional APTES-based layers.[40] The formed ethanol and/or other alcohols, depending on the plasma-induced cross-linking, are measured in ATR-FTIR, but they will evaporate under the high-vacuum conditions of the XPS measurements. Therefore, the hydrolysis process is one of the factors that result in the observed C-content decrease upon aging. The changes in the spectra due to hydrolysis are more significant than the changes due to oxidation, suggesting that the former process is occurring in a larger volume of the coating.

The ATR-FTIR and XPS measurements indicate that the applied power does not have a significant effect on the aging behavior of the AAPD-APTES coating in ambient air, within the employed power range. This seems to be in contrast with observations for PECVD, as plasma power is known to have a significant influence on the crosslinking degree, which can subsequently affect the aging properties of amine-rich plasma polymers.[60] Aziz *et al*, for example, observed a significant influence of the power on the wettability changes of coatings deposited by PECVD of allylamine, a primary amine-based precursor.[21] This could be the result of the differences between PECVD and AAPD, as mentioned before. But also other factors, such as the difference in between typical amine-based and aminosilane-based plasma polymer coatings, could influence this observation.[21, 35, 61-62] As such, it can be concluded

that more studies are needed to confirm the differences in terms of aging between AAPD- and PECVD-based coatings.

4. Conclusion

The present work was designed to study the differences in surface chemistry, wettability, morphology and aging between two APTES-based plasma polymer coatings. AAPD with APTES as precursor and APTES-modified ppHMDSO films were selected because of the limited available knowledge on the aging of both resulting coatings. WCA, ATR-FTIR and XPS showed that all coatings were deposited in a homogeneous way. These measurements also indicated that an increase in applied power did not have a significant influence on the chemistry and wettability of the AAPD-APTES films within the employed power range. These coatings had a complex organosilicon chemistry that contained a significant amount of alkoxysilane bonds, partially retained amines and a variety of oxidized functionalities, such as amides and carboxylic acids/esters. The XPS atomic composition of the ppHMDSO-APTES and AAPD-APTES coatings was similar, but the XPS high-resolution spectra revealed that the surface chemistry of the former coatings was different from the latter. The ppHMDSO-APTES coatings had a significantly higher amount of primary amines on its surface, while also the amount of intact Si-O-C-bonds was significantly lower. These observations were additionally supported by the aging study, in which a less significant amine protonation and more significant Si-O-C hydrolysis was observed for the AAPD-APTES coatings. In terms of surface morphology, AFM images illustrated that ppHMDSO-APTES layers had a similar morphology as the underlying UHMWPE substrate, although some sharp features with heights in the range of 100 - 400 nm were introduced onto the surface. For the AAPD-APTES coatings, the surface morphology was changed more significantly, but the underlying substrate could still be observed. XPS measurements after aging showed that protonation was the main involved process for the ppHMDSO-APTES coatings, while oxidation was involved to a lesser extent. For the AAPD-APTES layers, oxidation and hydrolysis were most important, which was supported by the FTIR measurements. The protonation of amines was less prevalent due to the low amount of these functionalities. Despite similar changes in the surface chemistry, the ppHMDSO-APTES coatings showed a significant change in wettability upon aging, while this surface property remained similar for the AAPD-APTES coatings. This can be attributed to the difference in cross-linking between both coatings, which has an influence on reorientation of polar functionalities. Comparing the chemistry and aging of the AAPD-APTES coatings highlighted that PECVD and AAPD are significantly different processes and that more knowledge should be gathered on the aging of AAPD-based coatings.

In conclusion, it can be asserted that this study provides useful comparative insights into the physicochemical properties and aging behavior of different APTES-based plasma polymers. This work can be used as a reference to decide which type of coating is preferred for a certain application and if aging needs to be minimized or not. Indeed, immobilization of biomolecules or nanoparticles might require a high primary amine density and can be performed under conditions that allow deprotonation of the coating, while improvement of adhesiveness is preferably performed under dry conditions. This makes the ppHMDSO-APTES coatings more interesting for the former application and the AAPD-APTES coatings for the latter. As such, further work should be performed to investigate the optimal usage of each coating for a specific application, which could additionally focus on the optimization of storage conditions and the mechanical durability of the coating. Other future work can also use the ppHMDSO-APTES coatings as a reference for further optimization of the AAPD-APTES coating deposition, in which the primary amine content can be increased by the addition of another gas in the discharge, for example.

5. Acknowledgments

Tim Egghe acknowledges the support of the Research Foundation Flanders (FWO) for a PhD grant strategic basic research (3S33118). Mehrnoush Narimisa acknowledges the support from the Special

Research Fund of Ghent University (Starting Grant; project number 01N00516). Rouba Ghobeira would like to thank the FWO (grant number 12ZC720N) for financing her post-doctoral position.

6. References

(1) Macgregor, M.; Vasilev, K. Perspective on Plasma Polymers for Applied Biomaterials Nanoengineering and the Recent Rise of Oxazolines. *Materials* **2019,** *12* (1), 191, DOI: 10.3390/ma12010191.

(2) Egghe, T.; Ghobeira, R.; Esbah Tabaei, P. S.; Morent, R.; Hoogenboom, R.; De Geyter, N. Silanization of Plasma-Activated Hexamethyldisiloxane-Based Plasma Polymers for Substrate-Independent Deposition of Coatings with Controlled Surface Chemistry. *ACS Applied Materials & Interfaces* **2022,** *14* (3), 4620-4636, DOI: 10.1021/acsami.1c18223.

(3) Egghe, T.; Cools, P.; Van Guyse, J. F. R.; Asadian, M.; Khalenkow, D.; Nikiforov, A.; Declercq, H.; Skirtach, A. G.; Morent, R.; Hoogenboom, R.; De Geyter, N. Water-Stable Plasma-Polymerized N,N-Dimethylacrylamide Coatings to Control Cellular Adhesion. *ACS Applied Materials & Interfaces* **2020,** *12* (2), 2116-2128, DOI: 10.1021/acsami.9b19526.

(4) Yasuda, H. Glow discharge polymerization. *Journal of Polymer Science: Macromolecular Reviews* **1981,** *16* (1), 199-293, DOI: 10.1002/pol.1981.230160104.

(5) Kylián, O.; Shelemin, A.; Solař, P.; Pleskunov, P.; Nikitin, D.; Kuzminova, A.; Štefaníková, R.; Kúš, P.; Cieslar, M.; Hanuš, J.; Choukourov, A.; Biederman, H. Magnetron Sputtering of Polymeric Targets: From Thin Films to Heterogeneous Metal/Plasma Polymer Nanoparticles. *Materials (Basel)* **2019,** *12* (15), 2366, DOI: 10.3390/ma12152366.

(6) Palumbo, F.; Lo Porto, C.; Fracassi, F.; Favia, P. Recent Advancements in the Use of Aerosol-Assisted Atmospheric Pressure Plasma Deposition. *Coatings* **2020,** *10* (5), 440.

(7) Van Guyse, J. F. R.; Cools, P.; Egghe, T.; Asadian, M.; Vergaelen, M.; Rigole, P.; Yan, W.; Benetti, E. M.; Jerca, V.-V.; Declercq, H.; Coenye, T.; Morent, R.; Hoogenboom, R.; De Geyter, N. Influence of the Aliphatic Side Chain on the Near Atmospheric Pressure Plasma Polymerization of 2-Alkyl-2-oxazolines for Biomedical Applications. *ACS Applied Materials & Interfaces* **2019,** *11* (34), 31356-31366, DOI: 10.1021/acsami.9b09999.

(8) Friedrich, J. F.; Mix, R.; Schulze, R.-D.; Meyer-Plath, A.; Joshi, R.; Wettmarshausen, S. New Plasma Techniques for Polymer Surface Modification with Monotype Functional Groups. *Plasma Processes and Polymers* **2008,** *5* (5), 407-423, DOI: 10.1002/ppap.200700145.

(9) Thiry, D.; Pouyanne, M.; Cossement, D.; Hemberg, A.; Snyders, R. Surface Engineering of Bromine-Based Plasma Polymer Films: A Step toward High Thiol Density Containing Organic Coatings. *Langmuir* **2018,** *34* (26), 7655-7662, DOI: 10.1021/acs.langmuir.8b01045.

(10) Chen, R. T.; Muir, B. W.; Such, G. K.; Postma, A.; Evans, R. A.; Pereira, S. M.; McLean, K. M.; Caruso, F. Surface "Click" Chemistry on Brominated Plasma Polymer Thin Films. *Langmuir* **2010,** *26* (5), 3388-3393, DOI: 10.1021/la9031688.

(11) Vandenbossche, M.; Hegemann, D. Recent approaches to reduce aging phenomena in oxygen- and nitrogen-containing plasma polymer films: An overview. *Current Opinion in Solid State and Materials Science* **2018,** *22* (1), 26-38, DOI: https://doi.org/10.1016/j.cossms.2018.01.001.

(12) Lecoq, E.; Duday, D.; Bulou, S.; Frache, G.; Hilt, F.; Maurau, R.; Choquet, P. Plasma Polymerization of APTES to Elaborate Nitrogen Containing Organosilicon Thin Films: Influence of Process Parameters and Discussion About the Growing Mechanisms. *Plasma Processes and Polymers* **2013,** *10* (3), 250-261, DOI: https://doi.org/10.1002/ppap.201200108.

(13) Gandhiraman, R. P.; Gubala, V.; Nam, L. C. H.; Volcke, C.; Doyle, C.; James, B.; Daniels, S.; Williams, D. E. Deposition of chemically reactive and repellent sites on biosensor chips for reduced non-specific binding. *Colloids and Surfaces B: Biointerfaces* **2010,** *79* (1), 270-275, DOI: https://doi.org/10.1016/j.colsurfb.2010.04.009.

(14) Volcke, C.; Gandhiraman, R. P.; Gubala, V.; Doyle, C.; Fonder, G.; Thiry, P. A.; Cafolla, A. A.; James, B.; Williams, D. E. Plasma functionalization of AFM tips for measurement of chemical interactions. *Journal of Colloid and Interface Science* **2010,** *348* (2), 322-328, DOI: https://doi.org/10.1016/j.jcis.2010.04.042.

(15) Alba-Elías, F.; Sainz-García, E.; González-Marcos, A.; Ordieres-Meré, J. Tribological behavior of plasma-polymerized aminopropyltriethoxysilane films deposited on thermoplastic elastomers substrates. *Thin Solid Films* **2013,** *540*, 125-134, DOI: https://doi.org/10.1016/j.tsf.2013.06.028.
(16) Da Ponte, G.; Ghosh, A. K.; Kakaroglou, A.; Van Hemelrijck, D.; Van Mele, B.; Verheyde, B. Adhesion Improvement between Epoxy and Stainless Steel Using a Silane Coupling Agent in an Atmospheric Plasma Process. *Plasma Processes and Polymers* **2015,** *12* (4), 347-361, DOI: https://doi.org/10.1002/ppap.201400106.
(17) Lachmann, K.; Dohse, A.; Thomas, M.; Pohl, S.; Meyring, W.; Dittmar, K. E. J.; Lindenmeier, W.; Klages, C. P. Surface modification of closed plastic bags for adherent cell cultivation. *The European Physical Journal - Applied Physics* **2011,** *55* (1), 13812, DOI: 10.1051/epjap/2011100467.
(18) Duday, D.; Vreuls, C.; Moreno, M.; Frache, G.; Boscher, N. D.; Zocchi, G.; Archambeau, C.; Van De Weerdt, C.; Martial, J.; Choquet, P. Atmospheric pressure plasma modified surfaces for immobilization of antimicrobial nisin peptides. *Surface and Coatings Technology* **2013,** *218*, 152-161, DOI: https://doi.org/10.1016/j.surfcoat.2012.12.045.
(19) Rao, X.; Abou Hassan, A.; Guyon, C.; Zhang, M.; Ognier, S.; Tatoulian, M. Plasma Polymer Layers with Primary Amino Groups for Immobilization of Nano- and Microparticles. *Plasma Chemistry and Plasma Processing* **2020,** *40* (2), 589-606, DOI: 10.1007/s11090-019-10056-z.
(20) Borris, J.; Thomas, M.; Klages, C. P.; Faupel, F.; Zaporojtchenko, V. Investigations into composition and structure of DBD-deposited amino group containing polymer layers. *Plasma Processes and Polymers* **2007,** *4* (S1), S482-486.
(21) Aziz, G.; Thukkaram, M.; De Geyter, N.; Morent, R. Plasma parameters effects on the properties, aging and stability behaviors of allylamine plasma coated ultra-high molecular weight polyethylene (UHMWPE) films. *Applied Surface Science* **2017,** *409*, 381-395, DOI: https://doi.org/10.1016/j.apsusc.2017.03.027.
(22) Swaraj, S.; Oran, U.; Lippitz, A.; Friedrich, J. F.; Unger, W. E. S. Aging of Plasma-Deposited Films Prepared from Organic Monomers. *Plasma Processes and Polymers* **2007,** *4* (S1), S784-S789, DOI: https://doi.org/10.1002/ppap.200731905.
(23) Gengenbach, T. R.; Griesser, H. J. Deposition conditions influence the postdeposition oxidation of methyl methacrylate plasma polymer films. *Journal of Polymer Science Part A: Polymer Chemistry* **1998,** *36* (6), 985-1000, DOI: https://doi.org/10.1002/(SICI)1099-0518(19980430)36:6<985::AID-POLA14>3.0.CO;2-H.
(24) Borek-Donten, J.; Nisol, B.; Filimon, M.; Lopes, M.; Collard, D.; Chassaing, M.; Cauchie, H.-M.; Heyberger, R. The industrial process for virucidal plasma coatings on textiles: From idea to upscaling. *Plasma Processes and Polymers* **2022,** (n/a), e2100249, DOI: https://doi.org/10.1002/ppap.202100249.
(25) Egghe, T.; Ghobeira, R.; Morent, R.; Hoogenboom, R.; De Geyter, N. Comparative study of the aging behavior of plasma activated hexamethyldisiloxane-based plasma polymers and silicone elastomer thin films. *Progress in Organic Coatings* **2022,** *172*, 107091, DOI: https://doi.org/10.1016/j.porgcoat.2022.107091.
(26) Alexander, M. R.; Short, R. D.; Jones, F. R.; Michaeli, W.; Blomfield, C. J. A Study of HMDSO/O2 Plasma Deposits Using a High-sensitivity and -energy Resolution XPS Instrument: Curve Fitting of the Si 2p Core Level. *Applied Surface Science* **1999,** *137* (1), 179-183, DOI: 10.1016/S0169-4332(98)00479-6.
(27) López, G. P.; Castner, D. G.; Ratner, B. D. XPS O 1s Binding Energies for Polymers Containing Hydroxyl, Ether, Ketone and Ester groups. *Surface and Interface Analysis* **1991,** *17* (5), 267-272, DOI: 10.1002/sia.740170508.
(28) Jagst, E. Surface Functional Group Characterization Using Chemical Derivatization X-ray Photoelectron Spectroscopy (CD-XPS). Berlin, 2011.
(29) Ben Said, S.; Arefi-Khonsari, F.; Pulpytel, J. Plasma Polymerization of 3-Aminopropyltrietoxysilane (APTES) by Open-Air Atmospheric Arc Plasma Jet for In-Line Treatments. *Plasma Processes and Polymers* **2016,** *13* (10), 1025-1035, DOI: https://doi.org/10.1002/ppap.201600079.

(30) Egghe, T.; Van Guyse, J. F. R.; Ghobeira, R.; Morent, R.; Hoogenboom, R.; De Geyter, N. Evaluation of cross-linking and degradation processes occurring at polymer surfaces upon plasma activation via size-exclusion chromatography. *Polymer Degradation and Stability* **2021,** *187*, 109543, DOI: https://doi.org/10.1016/j.polymdegradstab.2021.109543.
(31) Ramamoorthy, A.; Rahman, M.; Mooney, D. A.; Don MacElroy, J. M.; Dowling, D. P. Thermal stability studies of atmospheric plasma deposited siloxane films deposited on Vycor™ glass. *Surface and Coatings Technology* **2008,** *202* (17), 4130-4136, DOI: https://doi.org/10.1016/j.surfcoat.2008.03.003.
(32) Narimisa, M.; Krčma, F.; Onyshchenko, Y.; Kozáková, Z.; Morent, R.; De Geyter, N. Atmospheric Pressure Microwave Plasma Jet for Organic Thin Film Deposition. *Polymers* **2020,** *12* (2), 354.
(33) Truica-Marasescu, F.; Wertheimer, M. R. Nitrogen-Rich Plasma-Polymer Films for Biomedical Applications. *Plasma Processes and Polymers* **2008,** *5* (1), 44-57, DOI: 10.1002/ppap.200700077.
(34) Gueye, M.; Gries, T.; Noël, C.; Migot-Choux, S.; Bulou, S.; Lecoq, E.; Choquet, P.; Kutasi, K.; Belmonte, T. Interaction of (3-aminopropyl) triethoxysilane with pulsed Ar–O 2 afterglow: application to nanoparticles synthesis. *Plasma Chemistry and Plasma Processing* **2016,** *36* (4), 1031-1050.
(35) Gengenbach, T. R.; Griesser, H. J. Aging of 1,3-diaminopropane plasma-deposited polymer films: Mechanisms and reaction pathways. *Journal of Polymer Science Part A: Polymer Chemistry* **1999,** *37* (13), 2191-2206, DOI: https://doi.org/10.1002/(SICI)1099-0518(19990701)37:13<2191::AID-POLA34>3.0.CO;2-F.
(36) Nisol, B.; Poleunis, C.; Bertrand, P.; Reniers, F. Poly(ethylene glycol) Films Deposited by Atmospheric Pressure Plasma Liquid Deposition and Atmospheric Pressure Plasma-Enhanced Chemical Vapour Deposition: Process, Chemical Composition Analysis and Biocompatibility. *Plasma Processes and Polymers* **2010,** *7* (8), 715-725, DOI: 10.1002/ppap.201000023.
(37) Sloyan, K.; Lai, C.-Y.; Lu, J.-Y.; Alfakes, B.; Al Hassan, S.; Almansouri, I.; Dahlem, M. S.; Chiesa, M. Discerning the Contribution of Morphology and Chemistry in Wettability Studies. *The Journal of Physical Chemistry A* **2018,** *122* (38), 7768-7773, DOI: 10.1021/acs.jpca.8b04197.
(38) Aziz, G.; De Geyter, N.; Declercq, H.; Cornelissen, R.; Morent, R. Incorporation of amine moieties onto ultra-high molecular weight polyethylene (UHMWPE) surface via plasma and UV polymerization of allylamine. *Surface and Coatings Technology* **2015,** *271*, 39-47, DOI: 10.1016/j.surfcoat.2015.01.027.
(39) Socrates, G. *Infrared and Raman Characteristic Group Frequences: tables and charts*, John Wiley & Sons Ltd: 2001; Vol. 3.
(40) Pena-Alonso, R.; Rubio, F.; Rubio, J.; Oteo, J. Study of the hydrolysis and condensation of γ-Aminopropyltriethoxysilane by FT-IR spectroscopy. *Journal of materials science* **2007,** *42* (2), 595-603.
(41) Morent, R.; De Geyter, N.; Leys, C.; Gengembre, L.; Payen, E. Comparison between XPS- and FTIR-analysis of plasma-treated polypropylene film surfaces. *Surface and Interface Analysis* **2008,** *40* (3-4), 597-600, DOI: https://doi.org/10.1002/sia.2619.
(42) Thiry, D.; Konstantinidis, S.; Cornil, J.; Snyders, R. Plasma diagnostics for the low-pressure plasma polymerization process: A critical review. *Thin Solid Films* **2016,** *606*, 19-44, DOI: https://doi.org/10.1016/j.tsf.2016.02.058.
(43) Da Ponte, G.; Sardella, E.; Fanelli, F.; d'Agostino, R.; Gristina, R.; Favia, P. Plasma Deposition of PEO-Like Coatings with Aerosol-Assisted Dielectric Barrier Discharges. *Plasma Processes and Polymers* **2012,** *9* (11-12), 1176-1183, DOI: https://doi.org/10.1002/ppap.201100201.
(44) Morent, R.; De Geyter, N.; Van Vlierberghe, S.; Dubruel, P.; Leys, C.; Gengembre, L.; Schacht, E.; Payen, E. Deposition of HMDSO-based Coatings on PET Substrates Using an Atmospheric Pressure Dielectric Barrier Discharge. *Progress in Organic Coatings* **2009,** *64* (2), 304-310, DOI: 10.1016/j.porgcoat.2008.07.030.
(45) Morent, R.; De Geyter, N.; Van Vlierberghe, S.; Dubruel, P.; Leys, C.; Schacht, E. Organic–inorganic Behaviour of HMDSO Films Plasma-polymerized at Atmospheric Pressure. *Surface and Coatings Technology* **2009,** *203* (10), 1366-1372, DOI: 10.1016/j.surfcoat.2008.11.008.

(46) Zeng, X.; Xu, G.; Gao, Y.; An, Y. Surface Wettability of (3-Aminopropyl)triethoxysilane Self-Assembled Monolayers. *The Journal of Physical Chemistry B* **2011,** *115* (3), 450-454, DOI: 10.1021/jp109259b.
(47) Howarter, J. A.; Youngblood, J. P. Optimization of Silica Silanization by 3-Aminopropyltriethoxysilane. *Langmuir* **2006,** *22* (26), 11142-11147, DOI: 10.1021/la061240g.
(48) Zhu, M.; Lerum, M. Z.; Chen, W. How to Prepare Reproducible, Homogeneous, and Hydrolytically Stable Aminosilane-derived Layers on Silica. *Langmuir : the ACS journal of surfaces and colloids* **2012,** *28* (1), 416-423, DOI: 10.1021/la203638g.
(49) Smith, E. A.; Chen, W. How to prevent the loss of surface functionality derived from aminosilanes. *Langmuir : the ACS journal of surfaces and colloids* **2008,** *24* (21), 12405-12409, DOI: 10.1021/la802234x.
(50) Wang, W.; Vaughn, M. W. Morphology and Amine Accessibility of (3-Aminopropyl) Triethoxysilane Films on Glass Surfaces. *Scanning* **2008,** *30* (2), 65-77, DOI: 10.1002/sca.20097.
(51) Esbah Tabaei, P. S.; Ghobeira, R.; Cools, P.; Rezaei, F.; Nikiforov, A.; Morent, R.; De Geyter, N. Comparative Study Between In-plasma and Post-plasma Chemical Processes Occurring at the Surface of UHMWPE Subjected to Medium Pressure Ar and N2 Plasma Activation. *Polymer* **2020,** *193*, 122383, DOI: 10.1016/j.polymer.2020.122383.
(52) Van Vrekhem, S.; Vloebergh, K.; Asadian, M.; Vercruysse, C.; Declercq, H.; Van Tongel, A.; De Wilde, L.; De Geyter, N.; Morent, R. Improving the Surface Properties of an UHMWPE Shoulder Implant with an Atmospheric Pressure Plasma Jet. *Scientific Reports* **2018,** *8* (1), 4720, DOI: 10.1038/s41598-018-22921-6.
(53) Asenath Smith, E.; Chen, W. How To Prevent the Loss of Surface Functionality Derived from Aminosilanes. *Langmuir* **2008,** *24* (21), 12405-12409, DOI: 10.1021/la802234x.
(54) Rupper, P.; Vandenbossche, M.; Bernard, L.; Hegemann, D.; Heuberger, M. Composition and Stability of Plasma Polymer Films Exhibiting Vertical Chemical Gradients. *Langmuir* **2017,** *33* (9), 2340-2352, DOI: 10.1021/acs.langmuir.6b04600.
(55) Said, R. B.; Kolle, J. M.; Essalah, K.; Tangour, B.; Sayari, A. A Unified Approach to CO2–Amine Reaction Mechanisms. *ACS Omega* **2020,** *5* (40), 26125-26133, DOI: 10.1021/acsomega.0c03727.
(56) Min, H.; Girard-Lauriault, P.-L.; Gross, T.; Lippitz, A.; Dietrich, P.; Unger, W. E. S. Ambient-ageing Processes in Amine Self-assembled Monolayers on Microarray Slides as Studied by ToF-SIMS with Principal Component Analysis, XPS, and NEXAFS Spectroscopy. *Analytical and Bioanalytical Chemistry* **2012,** *403* (2), 613-623, DOI: 10.1007/s00216-012-5862-5.
(57) Vandencasteele, N.; Reniers, F. Plasma-modified polymer surfaces: Characterization using XPS. *Journal of Electron Spectroscopy and Related Phenomena* **2010,** *178-179*, 394-408, DOI: https://doi.org/10.1016/j.elspec.2009.12.003.
(58) De Geyter, N.; Morent, R.; Leys, C. Influence of ambient conditions on the ageing behaviour of plasma-treated PET surfaces. *Nuclear Instruments and Methods in Physics Research Section B: Beam Interactions with Materials and Atoms* **2008,** *266* (12), 3086-3090, DOI: https://doi.org/10.1016/j.nimb.2008.03.167.
(59) Weigel, C.; Kellner, R. FTIR-ATR-spectroscopic investigation of the silanization of germanium surfaces with 3-aminopropyltriethoxysilane. *Fresenius' Zeitschrift für Analytische Chemie* **1989,** *335* (7), 663-668.
(60) Dorst, J.; Vandenbossche, M.; Amberg, M.; Bernard, L.; Rupper, P.; Weltmann, K. D.; Fricke, K.; Hegemann, D. Improving the Stability of Amino-Containing Plasma Polymer Films in Aqueous Environments. *Langmuir* **2017,** *33* (40), 10736-10744, DOI: 10.1021/acs.langmuir.7b02135.
(61) Choukourov, A.; Biederman, H.; Kholodkov, I.; Slavinska, D.; Trchova, M.; Hollander, A. Properties of amine-containing coatings prepared by plasma polymerization. *Journal of Applied Polymer Science* **2004,** *92* (2), 979-990, DOI: https://doi.org/10.1002/app.13387.
(62) Manakhov, A.; Nečas, D.; Čechal, J.; Pavliňák, D.; Eliáš, M.; Zajíčková, L. Deposition of stable amine coating onto polycaprolactone nanofibers by low pressure cyclopropylamine plasma polymerization. *Thin Solid Films* **2015,** *581*, 7-13, DOI: https://doi.org/10.1016/j.tsf.2014.09.015.